Observations on Superfluid Meniscus in Rotating ^{3}He-B

H. Alles, J. P. Ruutu, A. V. Babkin, P. J. Hakonen, O. V. Lounasmaa, and E. B. Sonin*

Low Temperature Laboratory, Helsinki University of Technology, 02150 Espoo, Finland

(Received 7 November 1994)

The parabolic superfluid meniscus has been seen for states in which only (1) the normal or (2) the superfluid component of ^{3}He-B rotates. A reduced, temperature-dependent meniscus (1) was formed at small speeds $\Omega \lesssim 0.21$ rad/s. A deeper-than-expected meniscus (2) was observed after a rapid halt of the cryostat, when the normal fluid stops during a short relaxation time, followed by slow decay of the superfluid circulation. The depth of the meniscus (2) was explained by a reactive radial force between the rotating superfluid and the stationary normal liquid.

PACS numbers: 67.57.De

Observation of the classical parabolic meniscus of rotating ^{4}He-II provided the first evidence for the existence of superfluid vortices [1]. The two-fluid hydrodynamics of Landau predicted originally that only the normal part of the liquid would rotate and that, as a result, a reduction in the depth of the meniscus by a factor of ρ_n/ρ should occur. However, this has never been observed in ^{4}He because vortices appear in the bulk superfluid at very low critical angular velocities. In rotating superfluid ^{3}He-B, the vortex-free counterflow state (the Landau state) exists up to much higher speeds [2,3].

In ^{3}He-B, it is also possible that only the superfluid component rotates: After a rapid halt of spinning, the normal component decelerates very quickly because of its high viscosity. In contrast, the superfluid circulation, carried by vortices, decays during a much longer time which is determined by the dissipative mutual friction parameter B of vortices. The meniscus for such a state has never been observed experimentally or investigated theoretically until now.

In this Letter we report on interferometric studies of rotating superfluid ^{3}He-B. We have recorded optically surface profiles of liquid layers up to 1 mm thick and investigated the Landau state without vortices, as well as the state after a rapid stop of the cryostat during the comparatively slow decrease of superfluid circulation when the normal component is already at rest. A unique deeper-than-expected meniscus has been observed for the decaying, purely superfluid rotation. We present a theory which relates this enhanced meniscus to the reactive mutual friction parameter B'. Good agreement with our theory and the observed surface profile is obtained when previously determined values of B and B' [4], measured using an oscillating diaphragm, are employed.

Our apparatus is an advanced modification of the setup used in the first optical observations of superfluid ^{3}He [5]. The experimental cell, a copper cylinder with an inner radius $R = 10$ mm, was sealed from both ends by means of two fused silica windows. The symmetry axis is within 1 mm of the rotation axis. The liquid layer under investigation rests on a fused silica optical wedge inside the cell.

An expanded laser beam of 9 mm diameter illuminates the sample from above. Reflections from the free surface of the liquid and from the optical reference wedge produce an interference pattern which is focused by a single lens to the charge coupled device sensor of a cooled video camera [6], mounted inside the 4-K vacuum can of the dilution refrigerator. In order to increase the sensitivity for depth variations, the reference plane was deliberately tilted by 0.02° with respect to the horizon. Procedures for adjusting the optics as well as further experimental details will be described elsewhere [7].

At slow rotational speeds the curvature of the meniscus is small and it is difficult to reconstruct the actual surface profile from the fringes. A more sensitive method for comparison of different states is to follow the change in the liquid depth at the nadir of the speed-dependent paraboloid. By measuring the shift of fringes we were able to resolve changes in liquid depth within about 10 nm. The lateral length scale was calibrated against the meniscus of the normal liquid with $\Omega = 1.55$ rad/s at $T \gg T_c$.

Figure 1(a) displays an interferogram of a nonrotating horizontal liquid surface: The straight interference lines depict contours of equal depth. Rotation-induced curvature of the meniscus becomes evident from the interferograms as moving and bending fringes. At high speeds, when the slope of the free surface is comparable to the tilt of the reference plane, circular interference fringes are formed as is illustrated in Fig. 1(b), which presents the interferogram of a superfluid layer in steady rotation at $\Omega = 1.55$ rad/s.

The superfluid meniscus is determined by the balance between the pressure of the liquid and the gravitational force at the free surface: $z(r) = \delta P(r)/g\rho$. The pressure deviation $\delta P(r)$ is usually deduced from the momentum conservation law for the whole liquid: $P\delta_{ij} + \rho_s v_{si} v_{sj} + \rho_n v_{ni} v_{nj} =$ const. Assuming stationary uniform rotation at $\boldsymbol{v}_s = \boldsymbol{\Omega}_s \times \mathbf{r}$ and $\boldsymbol{v}_n = \boldsymbol{\Omega}_n \times \mathbf{r}$, one obtains for the

 0031-9007/95/74(14)/2744(4)$06.00

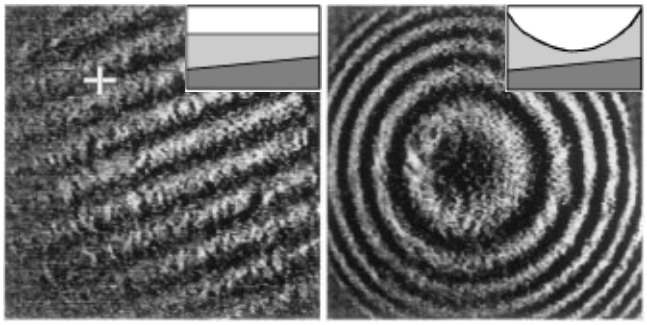

FIG. 1. Interferograms (20 ms long "snapshots") of (a) nonrotating and (b) rotating ($\Omega = 1.55$ rad/s) samples of ^{3}He-B. The adjacent fringes correspond to a change of 0.310 μm in liquid thickness above the tilted reference glass as is illustrated in the insets. The white cross in (a) defines the center of the optical cell. The displayed area of the interferograms in 5×5 mm^2.

surface profile

$$z(r) = \frac{1}{2g}\frac{\rho_s}{\rho}\Omega_s^2(r^2 - \tfrac{1}{2}R^2) + \frac{1}{2g}\frac{\rho_n}{\rho}\Omega_n^2(r^2 - \tfrac{1}{2}R^2). \quad (1)$$

Here we have also taken into account the constant-volume condition which states that the liquid level of a parabolic free surface in a rotating cylindrical container stays constant at $r = R/\sqrt{2}$. In the case of the equilibrium vortex state, $\Omega_s = \Omega_n = \Omega$, a classical parabolic meniscus is obtained, whereas for the Landau state, with $\Omega_s = 0$, Eq. (1) yields a meniscus reduced by the factor ρ_n/ρ.

In our experiments we have followed the level shift $\delta = |z(0)|$ which marks the vertical distance between the initial horizontal liquid level and the nadir of the Ω-induced paraboloid. Equation (1) yields depressions $\delta_{\mathrm{eq}} = \Omega^2R^2/4g$ and $\delta_n = (\rho_n/\rho)\Omega^2R^2/4g$ for the equilibrium vortex state and for the Landau state, respectively.

Figure 2 displays the rotation-induced level change δ of a 0.1 mm thick layer of ^{3}He-B at $T = 0.68T_c$. The data were obtained by measuring the shift of the interference fringes around the center of the cell [see Fig. 1(a)], while the speed of the cryostat was increased stepwise from rest. The acceleration rate was 0.01 rad/s^2, and "snapshots" were taken after the speed had been constant for 60 s at least. A clear jump of δ from the initial Ω^2 dependence (dashed curve) takes place when the angular velocity is increased above $\Omega_c \approx 0.20$ rad/s. The meniscus thus becomes suddenly deeper. All data points at lower speeds can be fitted well by Eq. (1) at $\Omega_s = 0$, with $\rho_n/\rho = 0.625$ taken from Ref. [8]. Thus we have a vortex-free superfluid state when $\Omega_c \lesssim 0.21$ rad/s, and the observed discontinuity in δ marks the creation of vortices in the sample. Above Ω_c the experimental points follow the full curve, drawn for "classical" behavior corresponding to the equilibrium density of vortices in the sample.

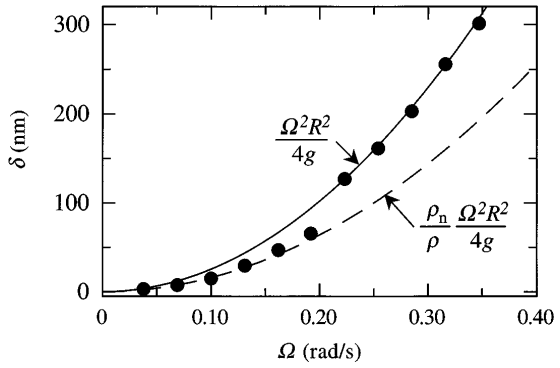

FIG. 2. Absolute change δ of the liquid height in the center of the Ω-induced parabola during acceleration as compared with the stationary free surface level for a 0.1 mm thick layer of ^{3}He-B. The solid and dashed curves mark the calculated behavior for a classical liquid and for a vortex-free superfluid with a flattened meniscus at $T = 0.68T_c$, respectively. Note the transition from the vortex-free behavior ($\boldsymbol{v}_n = \boldsymbol{\Omega} \times \mathbf{r}, \boldsymbol{v}_s = 0$) to the "classical" curve $\boldsymbol{v}_n = \boldsymbol{v}_s = \boldsymbol{\Omega} \times \mathbf{r}$ at $\Omega \approx 0.20$ rad/s. The size of the data points is approximately equal to the experimental error bars.

In order to study the relaxation of a vortex state, the cryostat was brought rapidly (within 1–1.5 s) to rest after steady rotation at $\Omega \gg \Omega_c$, applying simultaneously a series of light pulses to the sample. During the snapshot sequence the initially circular interference patterns [see Fig. 1(b)] changed first to curved fringes and later to almost straight lines [as in Fig. 1(a)] which was displaced from their equilibrium positions. We saw movement of the interference fringes in the superfluid for as long as 5–8 s after the cryostat had been brought to rest.

Figure 3 shows the surface profiles of a "rapid stopping" sequence performed on a 0.4 mm thick layer of ^{3}He-B at $T = 0.73T_c$. These curves were obtained after analyzing the interferograms recorded during deceleration of the cryostat linearly, in 1.2 s, from $\Omega = 1.55$ rad/s to

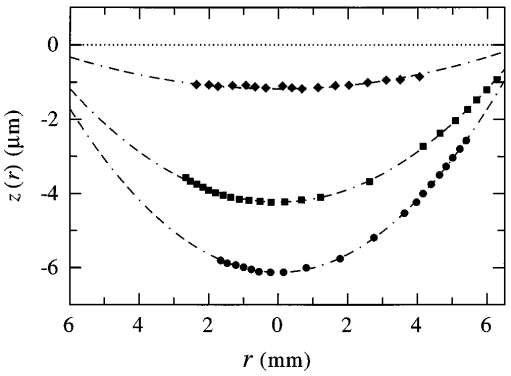

FIG. 3. Surface profiles from a "rapid stopping experiment," performed on a $d = 0.4$ mm thick layer of ^{3}He-B at $T = 0.76T_c$; r is the distance from the rotation axis. From *bottom* to *top*: snapshots at the speed $\Omega = 1.55$ rad/s, at $t = 0.2$ s, and $t = 0.8$ s after deceleration was started. The dotted line represents the horizontal free surface and the dash-dotted curves depict paraboloids fitted to the experimental points.

zero; the rate of applied laser pulses was 1.6 Hz. The influence of light was checked with a reference sequence on a stationary sample, which verified that the level rise due to the thermomechanical effect did not exceed 10 nm during the pulse sequence. Since the measured surface profiles are parabolic, the distribution of vorticity remains uniform during deceleration while the number of vortices decreases.

Our experimental data on relaxation of the meniscus at $T = 0.73T_c$ are presented in Fig. 4. The level change δ is plotted as a function of time, counting from the moment when deceleration of the cryostat was started. Initially the decrease in the depth of the meniscus was caused mostly by the normal liquid, which stops its rotation quickly when compared to the superfluid component. We estimate that there is no contribution to the meniscus from the normal fluid component after $t = 2.5$ s, i.e., 1.3 s after the complete stop of the cryostat. For this calculation we used the dispersion relation of thin film oscillations, Eq. (3) from Ref. [9]. We employed the values of the effective viscosity and thermal diffusion, which were obtained by extrapolation of our earlier data on the dynamics of thin ^{3}He-B films in the same experimental geometry (see Fig. 3 in Ref. [9]).

At $t > 2.5$ s the depth of the meniscus is solely governed by the rotating superfluid. The time dependence of the decaying superfluid vorticity can be expressed by the following nonlinear equation [10,11], viz.

$$\frac{\partial \Omega_s}{\partial t} + \frac{\rho_n}{\rho} B[\Omega_s^2 - \Omega(t)\Omega_s] = 0. \qquad (2)$$

Here the angular velocity of the cryostat Ω is time dependent and, at $t = 0$, the speed $\Omega_s(0) = \Omega(0)$. This model can be used when viscous relaxation is quick compared to changes in $\Omega(t)$, which then expresses the angular velocity of the normal liquid as well.

Recently Bevan *et al.* [4] have made extensive measurements on mutual friction in ^{3}He-B over a wide temperature range. We have drawn a dashed curve in Fig. 4, which is the solution of Eq. (2) for $T = 0.73T_c$, employing their measured value of $B\rho_n/\rho = 2.85$ at 1.6 bars; δ was calculated from Eq. (1) for $r = 0$ with $\Omega_n = 0$. Comparison of our data points with this curve indicates that the meniscus remains much deeper than predicted by Eq. (2).

In order to account for the observed deeper meniscus one must realize that the momentum conservation law does not apply in the decaying vortex state owing to a strong coupling of the thin normal-liquid layer with the bottom of the rotating container. Hence, the pressure deviation should be determined, instead, from the equation of the superfluid motion given by

$$\frac{\partial \boldsymbol{v}_s}{\partial t} + 2\boldsymbol{\Omega}_s \times \boldsymbol{v}_L + \boldsymbol{\nabla}(\mu_0 + \tfrac{1}{2} v_s^2) = 0. \qquad (3)$$

Here μ_0 is the chemical potential in a reference frame circulating with the superfluid velocity $\boldsymbol{v}_s$ at the given normal current $\rho_n(\boldsymbol{v}_n - \boldsymbol{v}_s)$ in the same frame and

$$\boldsymbol{v}_L = \boldsymbol{v}_s + \frac{\rho_n}{2\rho} B'(\boldsymbol{v}_n - \boldsymbol{v}_s) + \frac{\rho_n}{2\rho} B\hat{\boldsymbol{\Omega}} \times (\boldsymbol{v}_n - \boldsymbol{v}_s) \qquad (4)$$

is the vortex line velocity, determined by the Hall-Vinen mutual friction parameters B and B'. Note that Eq. (2) has been deduced by applying the operator $\boldsymbol{\nabla}\times$ to Eq. (3). By using the Gibbs-Duhem relation for small $\boldsymbol{v}_n - \boldsymbol{v}_s$,

$$\rho \delta\mu_0 = \delta P - S\delta T - \rho_n \frac{(\boldsymbol{v}_n - \boldsymbol{v}_s)^2}{2}, \qquad (5)$$

one obtains from the radial component of Eq. (3):

$$\delta P - S\delta T = \rho(\boldsymbol{v}_L \cdot \boldsymbol{v}_s) - \frac{\rho}{2} v_s^2 + \frac{\rho_n}{2}(\boldsymbol{v}_n - \boldsymbol{v}_s)^2. \qquad (6)$$

For an isothermal case ($\delta T = 0$), Eq. (6) is compatible with the relation $\delta P = \rho_s v_s^2/2 + \rho_n v_n^2/2$, derived from the momentum conservation law if vortices move with the center-of-mass velocity: $\boldsymbol{v}_L = (\rho_s/\rho)\boldsymbol{v}_s + (\rho_n/\rho)\boldsymbol{v}_n$. But for general vortex motion, the surface profile of an isothermal layer with the normal component at rest becomes

$$z(r) = \frac{\delta P(r)}{g\rho} = \frac{1}{g}\left[\left(1 - \frac{\rho_n}{2\rho} B'\right) - \frac{\rho_s}{2\rho}\right] \times \Omega_s^2(r^2 - \tfrac{1}{2}R^2), \qquad (7)$$

where we have taken the stationary liquid height as the reference level. Note that if B and B' are set equal to zero, the meniscus at $T > 0$ is different from the one given by Eq. (1), because in this case the vortex velocity $\boldsymbol{v}_L = \boldsymbol{v}_s$ does not coincide with the center-of-mass velocity.

The momentum conservation law is violated due to interaction of the liquid with the cell bottom via a weak viscous radial normal flow at the velocity v_{nr}. This produces an external force $\sim \eta_n v_{nr}/d^2$, which compensates the difference between the pressure variations determined from the momentum conservation law and from Eq. (6) using $\delta T = 0$. Here η_n is the dynamic shear

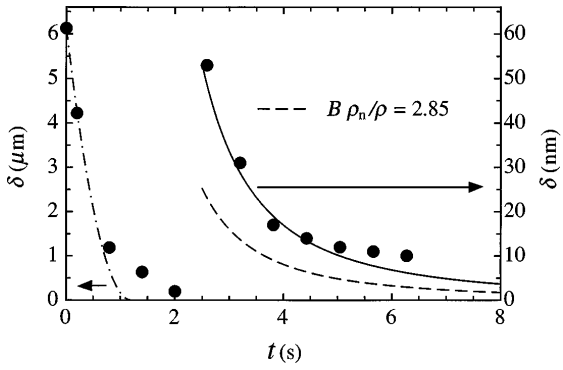

FIG. 4. Relaxation of the nadir in the Ω-induced parabola as a function of time during and after deceleration of the ^{3}He-B sample from the equilibrium vortex state at $\Omega = 1.55$ rad/s. Corresponding surface profiles for the first three data points are given in Fig. 3. Note that the right hand scale is magnified by 100×. The dash-dotted curve represents δ for the instantaneous speed of the cryostat during linear deceleration; for explanations of the other curves, see text.

viscosity, and d is the liquid layer thickness. On the other hand, the radial entropy flow $S v_{nr}$ is balanced by the thermal conductivity term $(\kappa/T)\partial T/\partial r$ and by the contribution from mutual-friction-induced dissipation $\sim(\rho_n\rho_s/\rho)B\Omega_s R v_s^2/T$. This results in a radial temperature variation which may be neglected in Eq. (6) if $d \ll \sqrt{\eta_n \kappa/S^2 T} \approx 1$ cm and $(S/\kappa)\rho_n\rho_s B\Omega_s R^2/\rho^2 \ll 1 - \rho_n B'/2\rho - \rho_s/2\rho$ (or $R^2 \ll 5$ cm^2 at $T = 0.7T_c$).

Using Eqs. (2) and (7), together with the values $B\rho_n/\rho = 2.85$ and $B'\rho_n/\rho = 1.05$ for $T = 0.73T_c$, taken from Ref. [4], we obtain good agreement with the observed relaxation of the meniscus (see solid line in Fig. 4). The reactive mutual friction parameter B' is thus responsible for the enhanced depth of the decaying meniscus by a factor of 2.1. In the temperature range of our experiments [$(0.7-0.8)T_c$], this deepening factor was found to be about 2 within our accuracy.

More systematic studies of mutual friction close to T_c, where this force is expected to increase, were impossible because the enhanced friction caused the superfluid to decay faster while the relaxation of the normal fluid component slowed down at the same time. As a result, a mixed state was observed close to T_c. As $T \to T_c$ one may expect that the superfluid velocity v_s cannot influence the fluid properties, i.e., $B'\rho_n/\rho \to 2$ in this limit, which agrees with the Manchester data on ^{3}He-B [4]. However, there are theories of ^{3}He-A [12] which predict that $2 - B'\rho_n/\rho = 0$, even at $T < T_c$. In this case, the meniscus in inverted according to Eq. (7). But there is no consensus on the value of $2 - B'\rho_n/\rho$ in ^{3}He-A; this difficulty is connected with the intrinsic angular momentum (see discussion in Sec. 10 of Ref. [13]).

In summary, we have succeeded in imaging two novel menisci in ^{3}He-B, not observed in superfluids before. At low rotational speeds a reduced meniscus was seen, which demonstrated the stationary Landau vortex-free state of the superfluid component. After a rapid stop of the cryostat an enhanced meniscus was detected, produced by the slowly decaying superfluid vorticity. Our theoretical analysis shows that such deepening of the meniscus is governed by the reactive mutual friction parameter B'; in fact, even an inverted meniscus might be possible in ^{3}He-A.

We want to thank A. Manninen for useful correspondence and the Manchester group for sharing their unpublished data. This work was financially supported by the Academy of Finland.

*Permanent address: Ioffe Physico-Technical Institute, St. Petersburg 194021, Russia.

[1] D. V. Osborne, Proc. Phys. Soc. London Sect. A **63**, 909 (1950); E. L. Andronikashvili and Yu. G. Mamaladze, Rev. Mod. Phys. **38**, 567 (1966).

[2] P. J. Hakonen and K. K. Nummila, Phys. Rev. Lett. **59**, 1006 (1987); J. M. Kyynäräinen, J. P. Pekola, K. Torizuka, A. J. Manninen, and A. V. Babkin, J. Low Temp. Phys. **82**, 325 (1991).

[3] J. S. Korhonen, A. D. Gongadze, Z. Janu, Y. Kondo, M. Krusius, Yu. M. Mukharsky, and E. V. Thuneberg, Phys. Rev. Lett. **65**, 1211 (1990); Y. Kondo, J. S. Korhonen, Ü. Parts, M. Krusius, O. V. Lounasmaa, and A. D. Gongadze, Physica (Amsterdam) **178B**, 90 (1992); P. J. Hakonen, Physica (Amsterdam) **178B**, 83 (1992).

[4] T. D. Bevan, A. J. Manninen, J. B. Cook, A. J. Armstrong, J. R. Hook, and H. E. Hall, Phys. Rev. Lett. **74**, 750 (1995).

[5] A. J. Manninen, J. P. Pekola, G. M. Kira, J. P. Ruutu, A. V. Babkin, H. Alles, and O. V. Lounasmaa, Phys. Rev. Lett. **69**, 2392 (1992).

[6] H. Alles, J. P. Ruutu, A. V. Babkin, P. J. Hakonen, A. J. Manninen, and J. P. Pekola, Rev. Sci. Instrum. **65**, 1784 (1994).

[7] H. Alles, J. P. Ruutu, A. V. Babkin, and P. J. Hakonen, J. Low Temp. Phys. (to be published).

[8] J. M. Parpia, D. G. Wildes, J. Saunders, E. K. Zeise, J. D. Reppy, and R. C. Richardsen, J. Low Temp. Phys. **61**, 337 (1985).

[9] J. P. Ruutu, H. Alles, A. V. Babkin, P. J. Hakonen, and E. Sonin, Europhys. Lett. **28**, 163 (1994).

[10] M. A. Alpar and K. S. Cheng, J. Low Temp. Phys. **60**, 415 (1985); P. J. Hakonen and V. P. Mineev, J. Low Temp. Phys. **67**, 313 (1987).

[11] M. Krusius, J. S. Korhonen, Y. Kondo, and E. B. Sonin, Phys. Rev. B **47**, 15 113 (1993).

[12] N. B. Kopnin, Phys. Rev. B **47**, 14 354 (1993); G. E. Volovik, Zh. Eksp. Teor. Fiz. **104**, 3070 (1993) [Sov. Phys. JETP **77**, 435 (1993)].

[13] E. B. Sonin, Physica (Amsterdam) **178B**, 106 (1992).